5

A panoptic model for planetesimal formation

S. Krijt, C. W. Ormel, C. Dominik, and A. G. G. M. Tielens
Astronomy & Astrophysics, to be submitted

Abstract

The journey from dust particle to planetesimal is a complex one, involving processes acting on very small scales (the physics governing the sticking and restructuring of porous aggregates) to the largest scales (the global structure of the turbulent protoplanetary nebula). Considering these processes simultaneously is essential when studying planetesimal formation. The goal of this work is to quantify where and when planetesimal formation can occur as the result of porous coagulation of realistic icy grains, and to understand how the process is influenced by the properties of the protoplanetary disk. We develop a novel, global, semi-analytical model for the evolution of the mass-dominating dust particles in a turbulent protoplanetary disk, that takes into account the evolution of the dust surface density, while preserving the essential characteristics of the porous coagulation process. The method is used to study the conversion of initially microscopic dust into planetesimals in disks around Sun-like stars. Disk parameters such as mass, size, metallicity, and temperature are varied to constrain regions where planetesimals can form, either through coagulation, or through inducing streaming instability (SI). For highly-porous ices, unaffected by collisional fragmentation and erosion, rapid growth to planetesimal sizes is possible in a zone stretching out to 20 AU for massive and dust rich disks. When porous coagulation is limited by erosive collisions, the formation of planetesimals through direct coagulation is not possible, but the creation of a large population of aggregates with Stokes numbers close to unity might trigger SI. We find that reaching conditions necessary for SI is possible in the inner regions of cold disks, or disks with a super-Solar

metallicity, but only if the turbulence is sufficiently weak. For perfectly sticking ices, planetesimal formation is a very efficient progress, and, depending on the turbulence strength, a significant fraction of the available dust mass is converted into planetesimals within 10^6 yrs. If growth is frustrated by erosive collisions, conditions suitable for SI could be reached for weakly turbulent disks, but the absence of dust pile-ups in the case of particles coagulating in a smooth nebula limits this possibility to either dust-rich or very cold disks.

5.1 Introduction

Protoplanetary disks are believed to be the sites of planet formation. In these disks, the coagulation of microscopic dust particles, already present in the interstellar medium, into kilometer-size planetesimals constitutes the first - and arguably least understood - step in the assembly of fully-grown planets (e.g., Testi et al. 2014; Johansen et al. 2014). Initially, the dust aggregates, held together by surface forces, grow by sticking to each other in gentle, low-velocity collisions (e.g., Kempf et al. 1999). As a result, aggregates form very open, porous structures. As the aggregates gain mass and their relative velocities increase, collisions become more energetic, leading to compaction and ultimately catastrophic fragmentation (Dominik & Tielens 1997; Blum & Wurm 2000). A second hurdle is presented in the form of the radial drift barrier: particles with certain aerodynamic properties decouple from the gas, and drift radially on short timescales (Whipple 1972; Weidenschilling 1977a; Brauer et al. 2008b).

In the inner few AU of the protoplanetary disk, dust grains consist mainly of silicates, and these aggregates bounce of each other in collisions, or even disrupt completely upon impact, at collision velocities above several m s^{-1} (Blum & Wurm 2008; Güttler et al. 2010). These collisional processes limit the growth beyond a centimeter or so in the inner disk (Brauer et al. 2008b; Zsom et al. 2010; Windmark et al. 2012a).

Outside the snow line, located typically at ~3 AU (Min et al. 2011), water ice becomes an important constituent of the dust grains. This is beneficial for growth, because aggregates composed of (mostly) ice are capable of sticking at tens of m s^{-1} (Wada et al. 2009, 2013; Gundlach & Blum 2015). In addition, these icy particles maintain highly-porous structures (Suyama et al. 2008, 2012), making them less likely to bounce in collisions (Wada et al. 2011; Seizinger & Kley 2013), and allowing them to out-grow the radial drift barrier in the inner ~10 AU of the protoplanetary nebula (Okuzumi et al. 2012; Kataoka et al. 2013a). However, the growth of these porous aggregates might be frustrated by high-velocity erosive collisions (Krijt et al. 2015).

Instead of coagulating directly, planetesimals can also be formed through particle concentration mechanisms (Johansen et al. 2014, and references thererin). One promising mechanism is the streaming instability (SI) (Youdin & Goodman 2005; Johansen et al. 2007; Bai & Stone 2010a,b), which can be triggered by creating a dense midplane layer of (partially) decoupled dust particles. Recently, Drążkowska & Dullemond (2014) have defined a set of conditions for SI, and compared them to dedicated models of compact coagulation. They found that in the inner disk, where the growth of silicates is limited by bouncing/fragmentation, particles can not grow to Stokes number large enough for trig-

gering SI. Outside the snow-line however, rapidly-growing highly-porous ice aggregates can grow to large Stokes numbers (Okuzumi et al. 2012), at which point their growth is possibly limited by erosive collisions (Krijt et al. 2015). The possibility of triggering SI through rapid porous coagulation has not yet been investigated, but the mass distributions obtained from erosion-limited porous growth appear very promising (Krijt et al. 2015).

We set out to study the formation of the first generation of planetesimals. Giant planets have not yet formed, hence the protoplanetary disk is smooth. We neglect possible presence of pressure bumps, dead zones, etc., and concentrate on the outer regions where ice dominates the sticking properties. The focus is to understand the evolution of the mass-dominating particles in disks around Sun-like stars, and understand how their evolution influences the dust surface density. Ultimately, the goal is to identify regions in both space and time where the first planetesimals can form, either through direct (porous) coagulation (e.g., Okuzumi et al. 2012) or through coagulation triggering SI (Drążkowska & Dullemond 2014). In order to answer these questions, we develop a global, semi-analytical, panoptic model that captures the evolution of the mass-dominating particles as they grow and drift radially in the protoplanetary disk.

The semi-analytical model is developed in Sect. 5.2. The method allows us to calculate the evolution of global dust surface density together with the masses and porosities of the growing dust particles, capturing processes such as porous growth, radial drift, bouncing/fragmentation and erosion in a way that is accurate as well as easy to follow. In Sect. 5.3 we use this model to study formation of planetesimals through direct coagulation, looking at both compact and porous growth. Then, in Sect. 5.4 we study under which conditions compact and porous growth can lead to conditions suitable for triggering SI. The results are discussed in Sect. 5.5 and the conclusions are summarized in Sect. 5.6.

5.2 Method

We consider a turbulent disk of gas around a $1M_\odot$ star, and focus on the region behind the snow line, where ices are an important part of the solid mass reservoir. The gas disk model (Sect. 5.2.1) assumes a smooth and static disk, with a mass that we will vary between $10^{-3} - 0.2M_\odot$. The method we will use for calculating the dust evolution is based on the semi-analytical model for porous growth of Krijt et al. (2015), which is combined with a new 'dust batch approach' that allows us to probe the evolution of the mass-dominating particles on a global scale, while preserving the essential characteristic of all porous growth process.

5.2.1 Nebula model

Following Lynden-Bell & Pringle (1974); Hartmann et al. (1998b), we adopt a truncated powerlaw for the surface density distribution

$$\Sigma_g = \Sigma_0 \left(\frac{R}{R_c}\right)^{-\gamma} \exp\left[-\left(\frac{R}{R_c}\right)^{2-\gamma}\right]. \tag{5.1}$$

We will vary the power law exponent between $\gamma = 3/2$, appropriate for the Minimum Mass Solar Nebula (MMSN) (Hayashi 1981); and $\gamma = 1$, consistent with observations (Andrews et al. 2009) and accretion disk theory (e.g. Armitage 2010). Disk masses and radii will be varied between $M_D = 10^{-3} M_\odot$ and $0.2 M_\odot$ and $R_c = 30 - 100$ AU, consistent with observational constraints for disks in the Taurus star forming region (Andrews & Williams 2005; Andrews et al. 2013). We adopt temperature structure appropriate for an optically thin disk around a solar type star

$$T = 125 \left(\frac{R}{5 \text{ AU}} \right)^{-1/2} \text{ K}, \tag{5.2}$$

appropriate for an optically thin disk, and in agreement with observational constraints (Andrews & Williams 2005). However, to probe the effect of the disk temperature, we will also consider colder disk models, in which the temperature is reduced by 50% with respect to Eq. 5.2.

Most other quantities are derived, together with assumptions about the turbulence and vertical structure, from Eqs. 5.1 and 5.2. The gas sound speed is given by

$$c_s = \sqrt{k_\text{B} T / m_g}, \tag{5.3}$$

with k_B the Boltzmann constant and $m_g = 3.9 \times 10^{-24}$ g for a mean molecular weight of 2.34. The Kepler frequency equals

$$\Omega = \sqrt{G M_\odot / R^3} = 1.8 \times 10^{-8} \left(\frac{R}{5 \text{ AU}} \right)^{-3/2} \text{ s}^{-1}. \tag{5.4}$$

Assuming an isothermal column, the gas density drops with increasing distance from the midplane z according to

$$\rho_g = \frac{\Sigma_g}{\sqrt{2\pi} h_g} \exp\left(\frac{-z^2}{2 h_g^2} \right), \tag{5.5}$$

with the vertical scale height of the gas $h_g = c_s / \Omega$. The turbulent viscosity is parametrized as $\nu_\text{turb} = \alpha c_s^2 / \Omega$ following Shakura & Sunyaev (1973).

5.2.2 Dust batch approach

At $t = 0$, we distribute a number of 'batches' of dust at different radii r_i in the protoplanetary disk. Each batch represents a swarm of dust particles with identical properties and growth histories. Typically, we will space the batches between 3 and 200 AU. Depending on the spacing of the batches, and the assumed dust density of the protoplanetary disk, a batch holds/represents a total dust mass M_i. The individual dust particles represented by a batch at any given time are assumed to be mono-disperse, and can be described by a particle mass m_i and a particle porosity ϕ_i. These four numbers (the total batch mass, batch location, and dust particle mass and porosity) fully describe the batch at time t. While M_i is constant in time, the other three properties vary in time. The location of the batch is

altered by radial drift, while the properties of the dust (so m_i and ϕ_i) evolve as the result of coagulation.

Using the locations and total masses of the batches, we define the cumulative dust mass

$$M_C(R) = \sum_{i,r_i<R} M_i, \tag{5.6}$$

which gives the total dust mass within a radius R. Using the cumulative mass, we can then obtain the dust surface density as

$$\Sigma_d(R) = \frac{1}{2\pi R} \frac{\mathrm{d}M_C(R)}{\mathrm{d}R}. \tag{5.7}$$

At $t = 0$, the r_i can be chosen arbitrarily (we will distribute them logarithmically), but their masses M_i are then fixed through Eqs. 5.6 and 5.7 and the assumed initial dust distribution. Initially, the dust density is set by the gas density, and $\Sigma_d/\Sigma_g = Z_0$, with $Z_0 \sim 10^{-2}$ the (vertically integrated) 'metallicity'. The dust is assumed to be in compact spherical monomers with radii a_0 and masses $m = m_0 = (4/3)\pi\rho_0 a_0^3$. Being compact spheres, monomers have $\phi = 1$. We use $\rho_0 = 1.4$ g cm^{-3} for icy particles and $\rho_0 = 2.6$ g cm^{-3} for silicate ones. As the batches evolve in time, dust masses and porosities change. In the rest of this section, we explain how we obtain $\dot{m}_i$, $\dot{r}_i$ and the evolution of ϕ_i.

5.2.3 Radial drift

As batches drift in, the radial density distribution batches changes, triggering a modification of the surface density. The radial drift velocity is given by (Weidenschilling 1977a)

$$\dot{r}_i = v_{\mathrm{drift}} = -\frac{2\Omega t_s}{1 + (\Omega t_s)^2} \eta v_{\mathrm{K}}, \tag{5.8}$$

where $v_{\mathrm{K}} = R\Omega$ is the Keplerian orbital velocity, and η can be written as (Nakagawa et al. 1986)

$$\eta \equiv -\frac{1}{2}\left(\frac{c_s}{v_{\mathrm{K}}}\right)^2 \frac{\partial \ln(\rho_g c_s^2)}{\partial \ln R}. \tag{5.9}$$

The drift timescale is defined as $t_{\mathrm{drift}} \equiv (r_i/\dot{r}_i)$ and depends on the masses and porosities of the dust particles through their dimensionless stopping time Ωt_s (see Appendix 5.A).

To test the treatment of radial drift, we run a model without coagulation. Dust particles are assumed to be compact micrometer icy spheres, in a disk with $\alpha = 10^{-3}$. Without coagulation, $\dot{m}_i = 0$ for all batches, and radial drift alone is responsible for changing the dust surface density. The results are shown in Fig. 5.1. Since, for a single grain size, Stokes numbers are largest in the outer part of the disk, particles further out will drift faster. As a result, the outer disk is slowly depleted of dust and pile-ups are created closer in. This picture is consistent with Youdin & Chiang (2004) and Birnstiel & Andrews (2014). The pile-ups are caused by the slowing down of particles as they drift into the more dense inner disk, and are the result of the assumption of a fixed (maximum) size

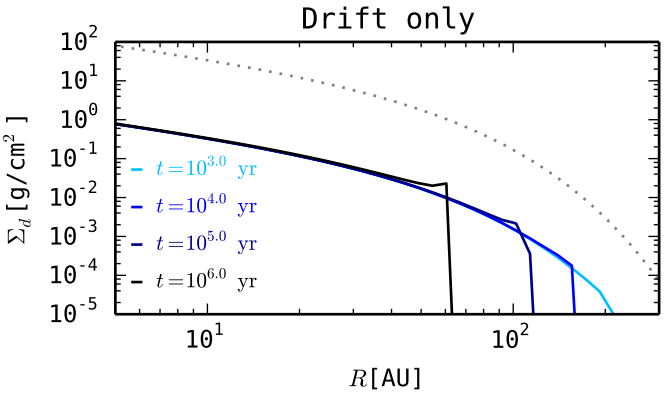

Figure 5.1: Evolution of the dust surface density for the case without coagulation: All dust particles are assumed to be compact micrometer-size silicate particles at all times. The initial metallicity equals $Z_0 = 0.01$ throughout the entire disk, and the dotted line shows the surface density of the gas corresponding to $M_D = 10^{-2} M_\odot$, $\gamma = 1$, and $R_c = 30$ AU.

of the particles. Below we will see that when grain sizes are limited by aerodynamical properties, no such pile-ups are created.

5.2.4 Porous coagulation

The model for porous coagulation is based on the semi-analytical model of Krijt et al. (2015, Sect. 5). Here, we briefly revisited the model, and describe how we take into account bouncing, fragmentation, and erosive collisions.

Growth timescales and porosity

For a mono-disperse dust population, the growth rate is given by

$$\dot{m}_i = \frac{\Sigma_d}{\sqrt{2\pi} h_d} \sigma_{\rm col} v_{\rm rel}, \tag{5.10}$$

with h_d the dust scale height, $\sigma_{\rm col}$ the collisional cross section, and $v_{\rm rel}$ the relative velocity between same-size dust particles. Appendix 5.B describes how the relative velocity is calculated. The growth timescale is then defined as

$$t_{\rm grow} \equiv \frac{m}{\dot{m}}. \tag{5.11}$$

The (relative) dust scale height is given by (Youdin & Lithwick 2007)

$$\frac{h_d}{h_g} = \left(1 + \frac{\Omega t_s}{\alpha} \frac{1 + 2\Omega t_s}{1 + \Omega t_s} \right)^{-1/2}. \tag{5.12}$$

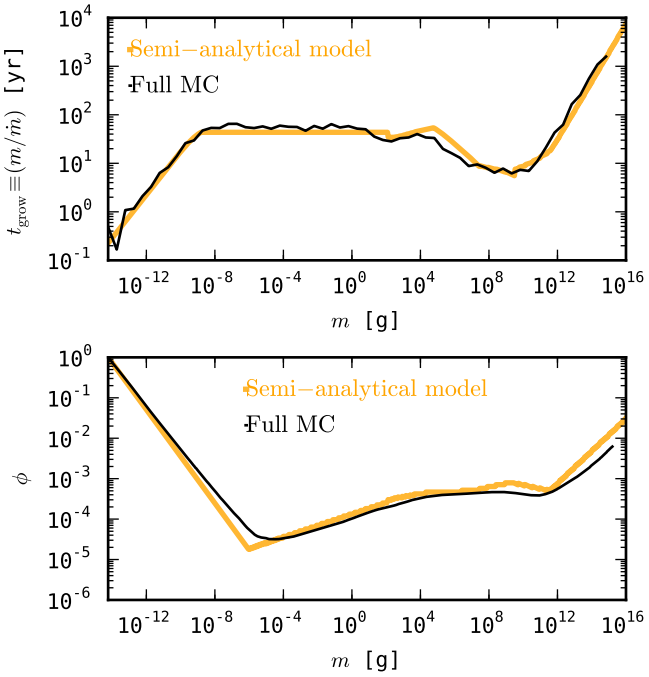

Figure 5.2: Comparison between semi-analytical model of Sect. 5.2.4 and full Monte Carlo (MC) model of Krijt et al. (2015) for icy aggregates coagulating locally at 5 AU in an MMSN disk with $\alpha = 10^{-3}$. Aggregates start as 0.1-μm monomers, and perfect sticking is assumed. *Top:* Growth timescale as a function of particle mass. *Bottom:* Volumetric filling factor as a function of mass.

The dust scale height depends on the particle Stokes number Ωt_s, with the stopping time t_s a function of the particle mass and porosity, and the local gas properties. The evolution of the particle porosity ϕ_i is not obtained with a time derivative. Instead, one can think of the porosity being set by the particle mass: $\phi_i = \phi(m_i)$. This is particularly true when the porosity is limited by gas compaction or self-gravity. Earlier in the evolution, the porosity is influenced predominantly by a dust particle's collisional history. Appendix 5.C describes the determination of $\phi(m_i)$ in more detail.

At the heart of the semi-analytical lies the assumption that the local dust population can be approximated by a mono-disperse grain population, with a single porosity. This assumption is valid when *i)* the full mass distribution has a clearly defined peak mass and porosity; and *ii)* the growth (and porosity-evolution, if dominated by collisions) of the peak-mass grains is mainly due to collisions with similar-size particles. These assumptions generally hold for populations resulting from porous coagulation (e.g., Ormel et al. 2007; Okuzumi et al. 2012; Krijt et al. 2015). To test assumption *ii)*, we compare the semi-analytical model the full Monte Carlo model of Krijt et al. (2015). For this comparison, drift is switched off ($\dot{r} = 0$), and perfect sticking is assumed. The results are shown

in Fig. 5.2. The trends in growth rates and internal density evolution obtained in from the full models are reproduced remarkably well by the semi-analytical model.

Bouncing, fragmentation, and erosion

Bouncing and fragmentation are modeled in the same way: by setting $\dot{m}_i = 0$ whenever the relative velocity between same-size particles exceeds the fragmentation or bouncing threshold velocity. Efficient erosion on the other hand, is taken into account by setting $\dot{m}_i = 0$ when the relative velocity between *dissimilar* particles exceeds the erosion threshold velocity. Specifically, we calculate the relative velocity between batch particles and single monomers, and compare that to the erosion threshold velocity.

When further growth is impeded by bouncing, fragmentation, or erosion, we will assume the dust particle porosity is constant in time as well. In the bouncing case in particular, this assumption might not be accurate because significant compaction through bouncing collisions is expected (Güttler et al. 2010; Zsom et al. 2010).

5.2.5 Combining drift and coagulation

Having tested drift and coagulation separately, we can now combine the two. To calculate drift and coagulation self-consistently, one needs to solve Eqs. 5.7, 5.8, and 5.10 simultaneously, while keeping track of the particle porosity in every batch. We do this by using a global time step Δt that is determined by the shortest drift- or growth-timescale present. We make sure $\Delta t \leq \min(0.5t_{\rm grow}, 0.05t_{\rm drift})$. In practice, this means one is limited by the (relatively short) growth timescales in the inner disk, until the dust there has drifted inside the snow line, cannot coagulate further because of destructive processes (bouncing/fragmentation or erosion), or has been converted into planetesimals.

Should the particle mass reach $m_i \geq m_p$, we call the particles planetesimals. At this point, we no longer calculate the evolution of these bodies, but rather treat the planetesimal formation process as finished. In this work, we will use $m_p = 10^{16}$ g, corresponding to a compact object of $\sim$ km in size. Once particles become planetesimals, we consider planetesimal formation to have been successful and set $\dot{m}_i = \dot{r}_i = 0$ for that batch. Also, their masses no longer contribute to Σ_d, but a separate planetesimal-surface-density Σ_p is calculated (a similar way as Σ_d in Eq. 5.7). Similarly, when a batch drifts inside of $R = R_{\rm min}$, we stop following it, since we are interested mainly in the region outside of the snow line. Conservatively, we place $R_{\rm min} = 1$ AU. We use between 10^2 and 10^3 batches per simulation. Using a larger number of batches did not result in significant changes of the resulting planetesimal populations.

5.3 Planetesimal formation through coagulation

For this section, we focus on the coagulation process and do not take into account effects of SI. To illustrate the difference between compact and porous growth, we first study the

coagulation of compact silicates (Sect. 5.3.1), and then discuss porous coagulation of ices in Sect. 5.3.2.

5.3.1 Compact growth

For compact growth, we start with submicron silicate particles and assume the porosity of the aggregates is always $\phi = 1$. In addition, we impose a fragmentation threshold velocity $v_{\rm frag} = 5$ m s^{-1} (Güttler et al. 2010; Wada et al. 2013). We assume a total disk mass of $M_D/M_\odot = 10^{-2}$, and (initial) metallicity of $Z_0 = 0.01$ throughout the disk[1]. The turbulence is constant throughout the disk and parameterized by $\alpha = 10^{-3}$.

The resulting surface density evolution is shown in the top panel of Fig. 5.3. At $t = 0$, the metallicity $Z_0 = 0.01$ throughout the disk, and the dust density follows the gas surface density (dotted line). After 10^3 yr not much has changed, as particles have not had enough time to grow large. After 10^4 and 10^5 yr, respectively, dust in the inner ∼10 and ∼30 AU has grown large enough to drift efficiently, and the inner regions become depleted in dust. Finally, after 10^6 yr the entire dust disk is depleted. Since the disk is smooth and cleared from the 'inside-out', no pile-ups are created, contrasting the fixed-size case of Fig. 5.1.

The bottom two panels of 5.3 show the 'lifelines' of a selection of dust batches for the same simulation. Dust particles start as monomers are 0.1 μm, and are evolved for 10^6 yr, close to the typical lifetime of a protoplanetary disk (Haisch et al. 2001). In Fig. 5.3, batches move *up* as their constituent grains gain mass, and to the *left* as they drift inward. The background colors show the history of porosities (middle panel) and Stokes number Ωt_s (bottom panel). Initially, particles couple well to the gas ($\Omega t_s \ll 10^{-3}$) and grow on relatively short timescales. Growth is faster in the inner disk, because both relative velocities and dust spatial densities are largest here. In the compact case however, an increase in particle mass inevitably results in a decrease of the surface-to-mass ratio, and the Stokes numbers increases. Aggregates with a mass of a few grams have $\Omega t_s \sim 1$, and drift inward rapidly. In addition, the largest particles in the inner ∼20 AU suffer from fragmentation, which limits their growth. This picture is as expected for compact growth, and the general trends are in good agreement with full models of compact coagulation (e.g., Okuzumi et al. 2012; Testi et al. 2014).

An alternative way of looking at the evolution of the dust is presented in Fig. 5.4. Here, the lifelines of the dust batches are plotted in terms of space and time. Green shaded regions indicate where $10^{-3} \leq \Omega t_s \leq 1$, and the letters denote current locations of Jupiter, Saturn, Uranus, and Neptune. While the individual lines do not give information about the masses and porosities of the dust particles making up the batch, it is clear growth is fastest in the inner disk, since the particles reach $\Omega t_s = 10^{-3}$ already after 10^3 yr. In the outer disk, around 100 AU, growth towards similar Stokes numbers takes almost 10^6 yr.

5.3.2 Porous growth

Here, we add the porosity evolution as described in Appendix 5.C. Because icy aggregates have high fragmentation threshold velocities (Dominik & Tielens 1997; Wada et al. 2013),

[1] A metallicity of $Z = 0.01$ is referred to as 'Solar'.

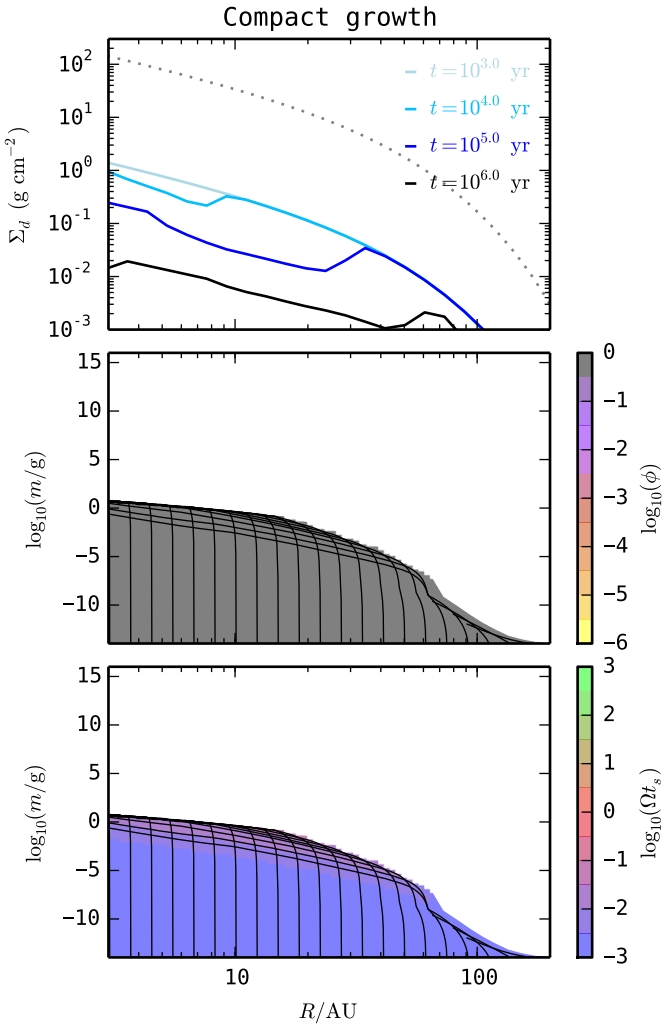

Figure 5.3: Coagulation of compact silicate particles with a fragmentation velocity of 5 m s^{-1}. The disk parameters were $M_D = 10^{-2} M_\odot$, $\gamma = 1$, and $R_c = 30$ AU. *Top:* Surface density evolution in time. The dotted line shows the gas surface density (Eq. 5.1), which is assumed to be static in time. *Middle:* Evolutionary histories of a selection of dust batches. Particles start out in the bottom of the plot as submicron-size monomers ($m \sim 10^{-14}$ g), and move up as they gain mass, and to the left as they drift inward. The background color indicates the porosity history of the grains. For compact coagulation, $\phi = 1$ at all times. *Bottom:* Similar to the middle panel, but now the colors indicate particle Stokes number. Bodies with $\Omega t_s \sim 1$ drift inward the fastest.

we do not include fragmentation. Recently however, Krijt et al. (2015) argued that erosion by small particles can be an effective way of halting growth when drift starts to play a

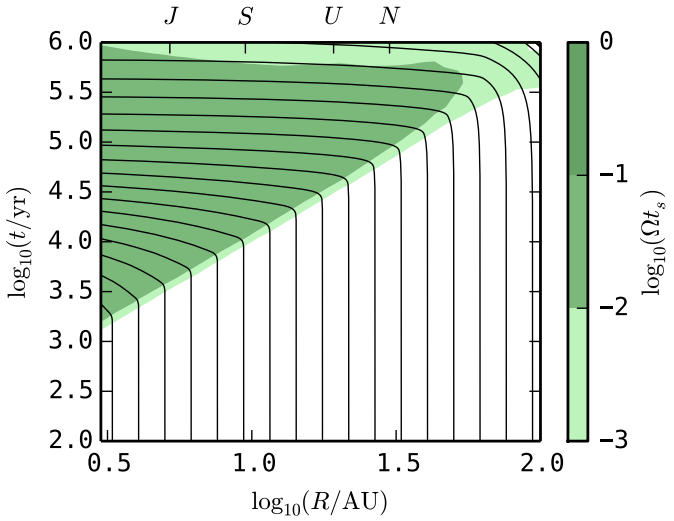

Figure 5.4: Evolution of dust batches in space and time for the model of Fig. 5.3 (compact growth with fragmentation at 5 m s^{-1}). Background colors show regions where particle Stokes numbers $10^{-3} \leq \Omega t_s \leq 1$.

role. Unfortunately, the threshold velocity above which erosion becomes significant is not accurately known for the highly-porous ice aggregates in question (see Krijt et al. 2015, Sect. 2.3.2.). Therefore, we will consider both cases: perfect sticking (Sect. 5.3.2), and effective erosion (Sect. 5.3.2).

Perfect sticking

Initially, we employ the same disk model as in the previous section, but because ice is added to the available solids, we start from $Z_0 = 0.02$. In Sects. 5.3.2 and 5.3.2, the effects of various disk parameters (e.g., total mass, size, and temperature) will be studied as well.

Fig. 5.5 shows the results for porous growth with perfect sticking. The top panel shows the surface density evolution in the case of porous growth. The solid lines correspond to Σ_d, and the dashed lines show Σ_p, the planetesimals. Aggregates in the inner disk (just outside the snow-line) can grow through the drift barrier, as found by Okuzumi et al. (2012); Kataoka et al. (2013a); Krijt et al. (2015), causing a pile up of solids around 5 AU, and a depletion of dust in the region further out. Although Okuzumi et al. (2012) used a different disk model and did not include gas- and self-gravity-compaction, this general picture is also obtained in their full global model (Okuzumi et al. 2012, Fig. 6). After 10^6 years, the entire disk is depleted in dust, and planetesimals have formed in the region just behind the snow line.

Focussing on the porosity (middle panel), we find that the porosities first decrease quickly as the result of hit-and-stick growth, and are then roughly constant due to collisional-

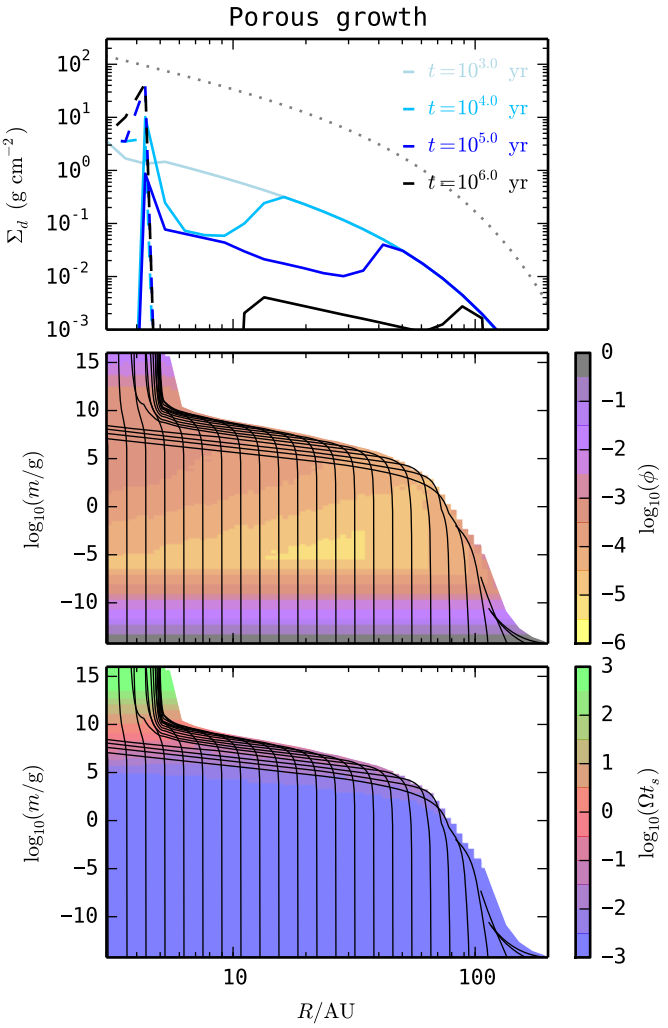

Figure 5.5: Porous growth with perfect sticking, for a disk with $M_D/M_\odot = 0.01$, $Z_0 = 0.02$, $R_c = 30$ AU, and $\gamma = 1$. *Top:* the surface densities of the gas (dotted), dust (solid), and planetesimals (dashed) are shown. *Middle:* Aggregates reach filling factors as low as 10^{-5}, before being compacted by gas ram pressure and collisions. *Bottom:* In the inner disk, aggregates can out-grow the radial drift barrier, and form massive, relatively compact, planetesimals with $\Omega t_s > 10^3$.

and (mostly) gas-compaction. For bodies with $m > 10^{12}$ g, self-gravity dominates the porosity and the filling factor increases to $\sim 10^{-1}$, consistent with Fig. 5.2, Kataoka et al. (2013a) and Krijt et al. (2015).

The bottom panel of Fig. 5.5 illustrates how aggregates grow through the radial drift

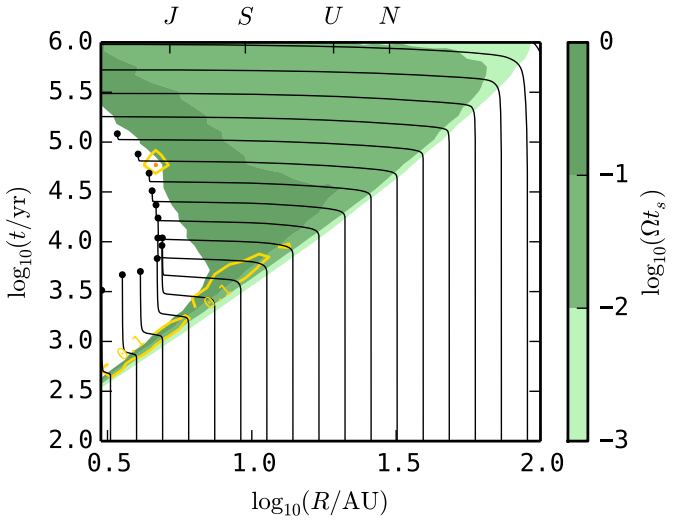

Figure 5.6: Evolution of dust batches in time for the simulation of Fig. 5.5 (porous growth with perfect sticking). The •-symbols indicate planetesimal formation through coagulation, and contours depict the midplane dust-to-gas ratio of particles with high Stokes numbers (see Sect. 5.4). For this particular disk model, planetesimal can form out to ∼5 AU.

barrier. Initially, aggregates grow through hit-and-stick collisions and their surface-to-mass ratio hardly changes (cf. Fig. 5.2). As a result, the aggregates' Stokes number stays $\ll 1$ while the mass increases over many orders of magnitude. Only when masses $>10^5$ g do particles start to experience substantial drift. In the inner disk, $\Omega t_s = 1$ corresponds to $m \sim 10^9$g (Krijt et al. 2015, Fig. 8). However, we also see particles with masses $10^7 - 10^8$ drifting to radii <3 AU. These tracks belong to particles that started out in the outer disk, and spent a lot of time in the early growth phase. By the time they started to drift and reached the inner disk, the dust surface density was already significantly decreased, making it difficult for the newly-arrived aggregates to grow since $\dot{m} \propto \Sigma_d$ (Eq. 5.10). Since planetesimals do not contribute to Σ_d, they do not influence the evolution of the drifting dust particles. This assumption is discussed further in Sect. 5.5.

In Fig. 5.6, the results of the porous coagulation model are plotted in a similar way as Fig. 5.4. The black solid spheres correspond to successful planetesimal formation through coagulation (i.e., $m_i \geq 10^{16}$ g). For this particular gas disk model, planetesimals can be seen to form out to ∼5 AU (cf. Fig. 5.5). In the inner disk, where the aggregates out-grow the radial drift barrier, the aggregates spend very little time having $10^{-3} \leq \Omega t_s \leq 1$. Again, we see that particles that start out in the outer disk take much longer to start drifting, and eventually drift through the planetesimal populations after $\sim 10^5$ yr.

Total planetesimal mass

By keeping track of the total mass of batches that have been converted into planetesimals, we obtain the total planetesimal mass as a function of time. Fig. 5.7 plots this mass $\Sigma m_{\rm pl}$ as a function of time for a grid of models with different disk masses and initial metallicities. All disks shared $\alpha = 10^{-3}$ and $R_c = 30$ AU. Most planetesimals form in the first 10^5 yrs, and it is clear that both a higher disk mass, and a higher initial metallicity lead to a larger total mass of planetesimals. For disk masses between 0.01 and 0.2 $M_\odot$, and metallicities between $Z_0 = 0.01 - 0.05$, between 10 and $\sim 10^3 M_\oplus$ of planetesimals can form through porous coagulation. These masses represent a considerable fraction of the total dust mass that is present in the disk.

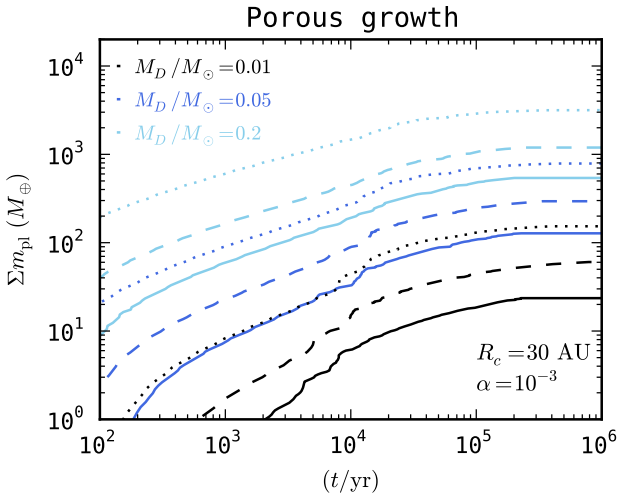

Figure 5.7: Total mass of planetesimals as a function of time for porous growth without erosion. Different linestyles indicate $Z_0 = 0.01$ (solid); $Z_0 = 0.02$ (dashed); and $Z_0 = 0.05$ (dotted). The total planetesimal mass increases significantly with disk mass and disk metallicity.

The top panel of Fig. 5.8 shows the same results but normalized to the total available dust mass $Z_0 M_D$. All disks considered here convert over 70% of their dust to planetesimals within a million years. Dust-rich, massive disks are most efficient, with an efficiency of ~90% after 10^6 yrs. The middle and bottom panel of Figure 5.8 show similar plots for more extended protoplanetary disks ($R_c = 100$ AU), with $\alpha = 10^{-3}$ and 10^{-5}, respectively. An increased physical size of the protoplanetary disk causes a decrease in the planetesimal-formation efficiency. In addition, a lower turbulence strength leads to slower growth, and $\Sigma m_{\rm pl}/(Z_0 M_D)$ reaches only 0.2-0.5 within 10^6 yr, depending on the disk parameters.

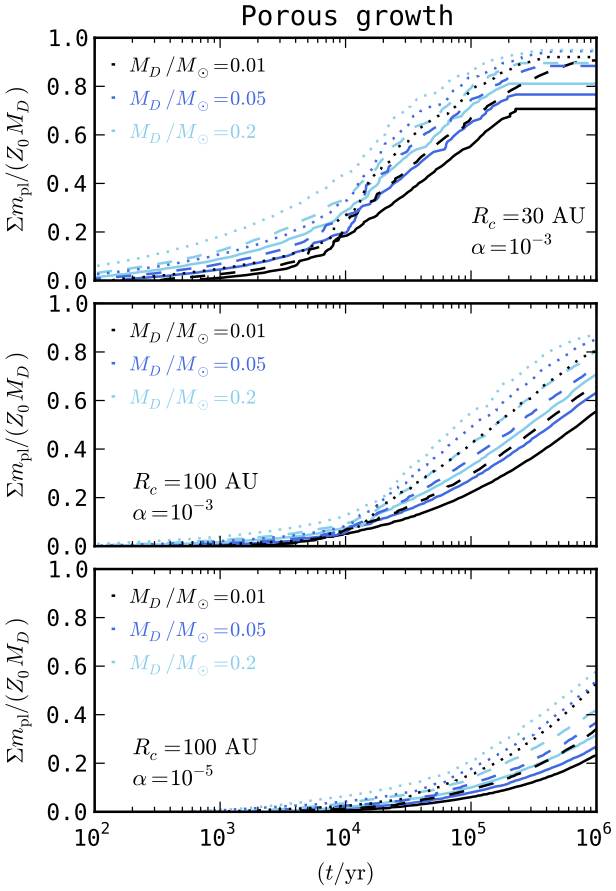

Figure 5.8: Fraction of total dust mass $Z_0 M_D$ that has been converted into planetesimals as a function of time, for different disk models. *Top:* MMSN-like disk with $\alpha = 10^{-3}$. *Middle:* More extended and shallower disk, also with $\alpha = 10^{-3}$. *Bottom:* The same extended disk, but with a weaker turbulence ($\alpha = 10^{-5}$). In general, porous growth in combination with perfect sticking is a very efficient way of turning dust into planetesimals; the efficiency being highest for disks with a high initial dust content. Weaker turbulence results in slower growth.

Planetesimal formation region

The size of the zone where aggregates can out-grow the radial drift barrier depends on disk parameters as well. Fig. 5.9 shows how the outer edge of this 'planetesimal formation zone' varies with total disk mass and metallicity for a compact disk (R_c = 30 AU, dotted), and a more extended disk (R_c = 100 AU, solid).

This dependency on disk mass was also noted by Okuzumi et al. (2012), and results from both a high dust density, and a lower gas molecule mean free path $\lambda_{\rm mfp}$; the length of

the mean free path (together with the aggregate's size) determines in which drag regime the aggregates are situated, and has a large impact on the growth timescale (see Sect. 5.A and Okuzumi et al. 2012). An increased metallicity directly results in a larger local dust density, making it easier for dust particles to outgrow radial drift, also increasing the size of the planetesimal formation zone. The planetesimal belt is somewhat larger for compact disks than for extended ones with identical total mass. The reason is that, for a given total disk mass, a smaller R_c leads to a higher dust surface density at radii $R < R_c$, and the higher the local dust surface density, the easier it becomes to outgrow radial drift. Comparing the distances to the current locations of the planets in our Solar System, we find that massive disks ($M_D/M_\odot = 0.2$) with a high dust content ($Z_0 = 0.05$) can form planetesimals as far out as ∼20 AU, or the current location of Uranus. Figure 5.10 shows the impact of varying the slope of the surface density power law γ, and the disk temperature. An increase in γ has a similar effect as a decrease in R_c: mass becomes more concentrated in the inner disk, resulting in a smaller planetesimal formation zone. Cold disks are flatter (smaller h_g), and have a lower maximum drift velocity ηv_K. The combined effects of lowering the temperature by a factor 2 with respect to Eq. 5.2 has a tremendous impact, increasing the outer edge of the planetesimal belt by almost a factor of 2.

At small radii, the icy particles needed for porous and perfect-sticking growth might not be present. The snow line, inside of which temperatures are too high to allow for water ice to be present, typically lies at ∼3 AU, but varies with turbulence strength and accretion rate (Min et al. 2011). The gray shaded area in Figs. 5.9 and 5.10 indicate the region within 3 AU. The assumption that dust particles are not destroyed in collisions is expected to break down in this region. Thus, low-mass disks ($M_D \sim 10^{-3} M_\odot$) might bot be able to form planetesimals through direct coagulation. Finally, while we only consider grain growth by coagulation, growth by water vapor condensation can be an efficient way of gaining mass close to the snow line (Cuzzi & Zahnle 2004; Ros & Johansen 2013), locally enhancing the growth rates.

Erosion-limited growth

In the previous section we have assumed perfect sticking for the highly-porous icy aggregates. Now, to mimic the effect of efficient erosion, we set $\dot{m}_i = 0$ whenever the relative velocity between the dust particles in the batch and monomers exceeds some erosion threshold velocity. The best data on erosion of icy particles comes from Gundlach & Blum (2015), who measured an erosion threshold velocity of ∼15 m s^{-1} for aggregates composed of (sub)micron-size monomers.

Fig. 5.11 shows the results for the same model as Fig. 5.5, but now including an erosion threshold velocity of 20 m s^{-1}. For low Stokes numbers, collision velocities are too low to cause erosion, and growth proceeds similarly to Fig. 5.5. Then, as aggregates grow towards $\Omega t_s \sim 1$, the collision velocity with small, well-coupled monomers approaches the maximum drift velocity of $\sim \eta v_K$, which is well above 20 m s^{-1} for this particular disk model. Erosion, assumed to be efficient, then acts to halt further growth, and prevents formation of planetesimals through direct coagulation. Since coagulation is fastest in the

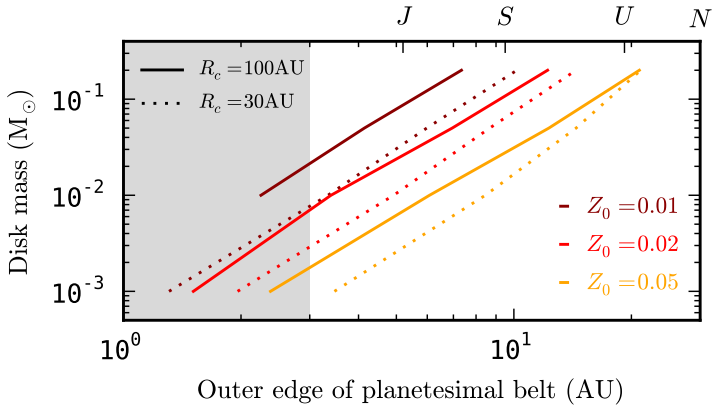

Figure 5.9: Outer edge of planetesimal formation zone as a function of disk mass M_D and initial metallicity Z_0, assuming R_c = 100 AU (solid); and R_c = 30 AU (dotted). Letters refer to the (current) locations of Jupiter, Saturn, Uranus and Neptune. For more massive, and more dust-rich disks, the planetesimal formation zone extends further out.

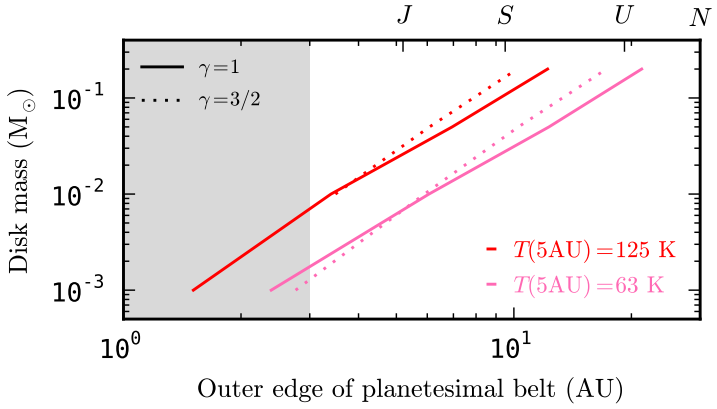

Figure 5.10: The effect of disk temperature and surface density exponent on the size of the planetesimal formation zone, for a fixed metallicity Z_0 = 0.02 and R_c = 100 AU. The effect of varying γ is small compared to the effect of reducing the temperature by 50%.

inner regions of the disk, erosion-limited growth results in an inside-out removal of the dust (similar to what was found for fragmentation-limited compact growth of Fig. 5.3). At later times, a sharp drop in Σ_d can be observed in Fig. 5.11 around $R \sim 5$ AU. This sudden drop in dust surface density is an artifact of the dust batch approach and can occur when, as a result of drift, the dust population in the dust-depleted region is represented by a small number of batches (see Sect. 5.5.1).

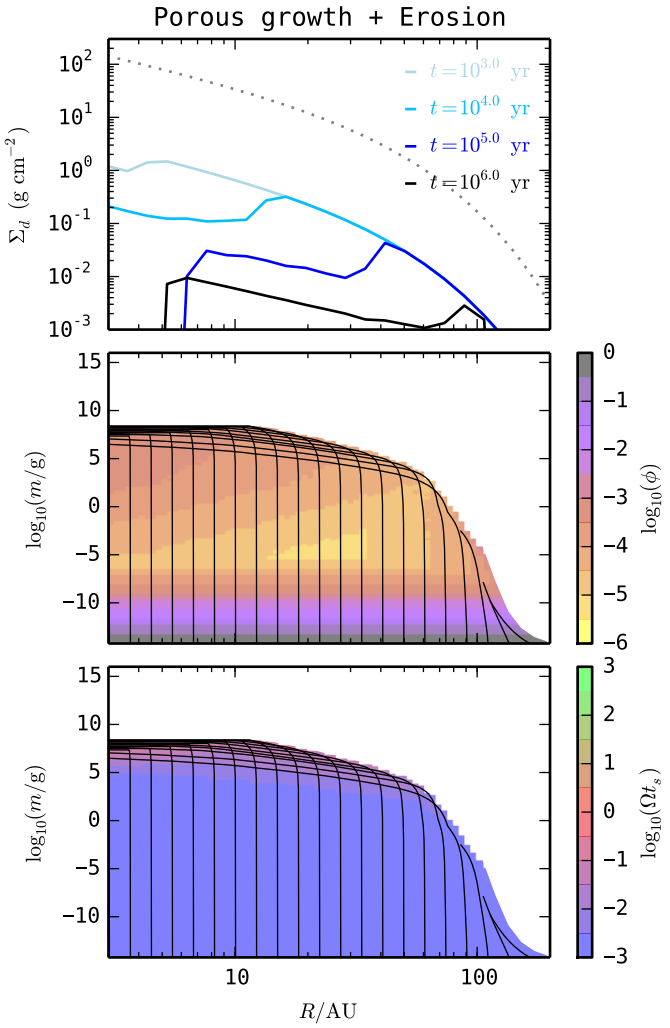

Figure 5.11: Porous growth followed by erosion. Dust and disk models are the same as in Fig. 5.5, but with efficient erosion above drift velocities of 20 m s^{-1}.

5.4 Planetesimal formation through SI

In addition to coagulating directly, planetesimals can also form through streaming instability (SI) (e.g., Youdin & Goodman 2005; Johansen et al. 2007; Bai & Stone 2010a,b). In this section, we investigate how coagulation (both compact and porous) can lead to conditions suitable for triggering SI.

5.4.1 Conditions for SI

We make use of the work of Drążkowska & Dullemond (2014), who, based on the work of Johansen et al. (2007, 2009); Bai & Stone (2010a,b) defined three conditions for triggering SI. For a mono-disperse particle distribution, these conditions are equivalent to:

i) The Stokes number of the mass dominating particles needs to be close to unity; specifically, $10^{-2} \leq \Omega t_s \leq 1$;

ii) The midplane dust-to-gas ratio of these particles needs to exceed, or be close to, unity;

iii) The vertically integrated metallicity should be a few times Solar;

Lastly, SI needs time to develop and will not be triggered if the growth timescales of the particles are too short. Thus, we add a final condition:

iv) The growth timescale needs to be longer than the timescale for SI instability to develop: $t_{\rm grow} > \Omega^{-1}$.

The first two conditions are related to efficient momentum transfer between dust particles and the gas. Particles with much higher Stokes numbers do not effectively interact with the gas, while particles with with much smaller stopping times do not result in strong clumping. Conditions *iii)* is related to supressing midplane turbulence. For high metallicities, the strength of this turbulence drops sharply (Bai & Stone 2010a).

We focus on conditions *i)*, *ii)*, and *iv)*, and address *iii)* in Sect. 5.4.4. Armed with the semi-analytical model of Sect. 5.2, we can now identify regions in space and time where these conditions are met. We will look at compact coagulation first, and then turn to porous coagulation. We define the midplane dust-to-gas ratio of decoupled particles as $(\rho_d^*/\rho_g)_{z=0}$, where the asterisk indicates that only particles with $10^{-2} \leq \Omega t_s \leq 1$ contribute to the dust density. For a mono-disperse particle distribution

$$(\rho_d^*/\rho_g)_{z=0} = \frac{(\Sigma_d/h_d)^*}{\Sigma_g/h_g} = Z^* \frac{h_g}{h_d}, \tag{5.13}$$

where the dust scale height depends on the particle Stokes number through Eq. 5.12.

5.4.2 Compact coagulation

For compact particles, Drążkowska & Dullemond (2014) find that bouncing and fragmentation prevent particles from growing to $\Omega t_s > 10^{-2}$, making the condition *i)* of Sect. 5.4.1 hard to fulfill. In our compact model, shown in Fig. 5.4, particles did reach high enough Stokes numbers; the reason is that we used a (rather optimistic) bouncing/fragmentation threshold of 5 m s^{-1}, while Drążkowska & Dullemond (2014) used 0.1 m s^{-1}. To test the influence of the threshold velocity, we ran a model identical to the earlier compact coagulation one, but now assuming a growth barrier for velocities above 1 m s^{-1}; the results are shown in Fig. 5.12. While there is a large region in the disk where the mass-dominating

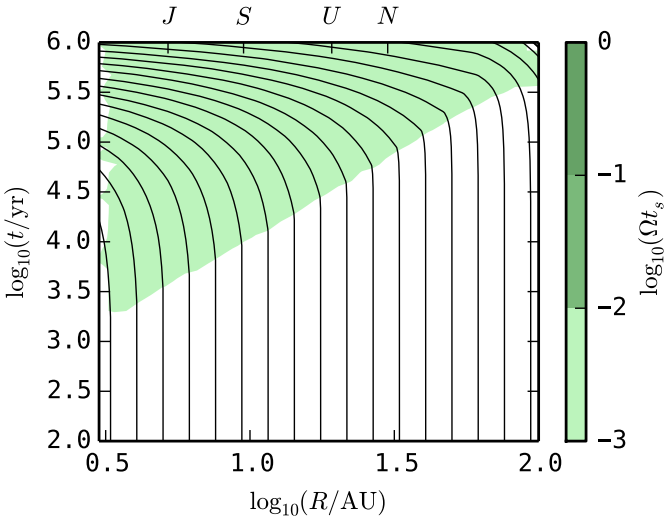

Figure 5.12: Evolution of dust batches assuming compact coagulation with a fragmentation/bouncing threshold velocity of 1 m s^{-1}. A compact $10^{-2} M_\odot$ disk was assumed, with initial metallicity $Z_0 = 0.01$ and $\alpha = 10^{-3}$. Compact particles do not reach $\Omega t_s > 10^{-2}$, and the dust-to-gas ratio in the midplane never exceeds 10^{-1}.

particles have $\Omega t_s > 10^{-3}$, the combination of drift and bouncing/fragmentation prevents particles from growing to Stokes numbers sufficient for SI.

The Stokes number at which particles fragment as a result of turbulence equals (e.g., Birnstiel et al. 2009)

$$(\Omega t_s)_{\max} \simeq \alpha^{-1} \left(\frac{v_{\mathrm{frag}}}{c_s} \right)^2, \tag{5.14}$$

with v_{frag} the fragmentation velocity. At 5 AU, assuming the temperature structure of Eq. 5.2, this leads to $(\Omega t_s)_{\max} \sim 10^{-3}$ for $v_{\mathrm{frag}} = 1$ m s^{-1} and $\alpha = 10^{-3}$. For low turbulence strengths, the relative velocities come from differential drift, resulting in (e.g., Birnstiel et al. 2012)

$$(\Omega t_s)_{\max} \simeq \frac{v_{\mathrm{frag}}}{\eta v_{\mathrm{K}}}, \tag{5.15}$$

with $\eta v_{\mathrm{K}} \simeq 50$ m s^{-1} in an MMSN-disk.

5.4.3 Porous coagulation

For ices, v_{frag} is much larger, several tens of m s^{-1} (Dominik & Tielens 1997; Wada et al. 2013), and growth to larger Stokes numbers is possible. Focussing on the perfect sticking case first, Fig. 5.6 shows that condition *i)* is fulfilled in a large part of the protoplanetary disk. In the inner disk however, growth *through* the drift barrier is so rapid, that aggregates

spend very little time having Stokes numbers that are suited for triggering SI (Okuzumi et al. 2012, Sect. 5.2.2.). As a result, condition *iv)* is not met in the inner disk.

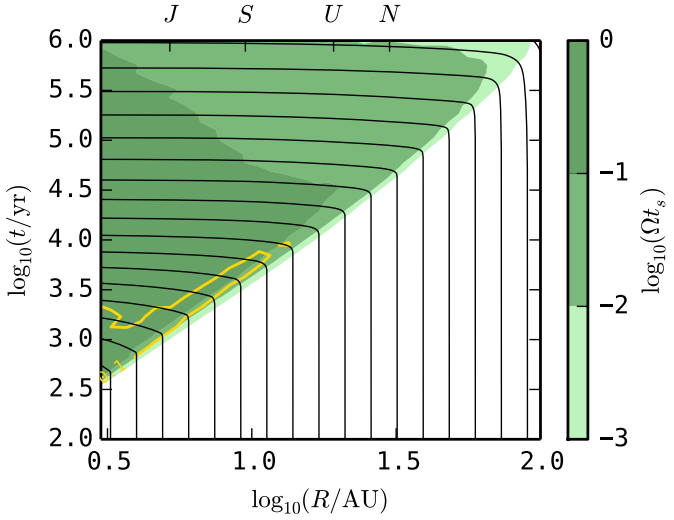

Figure 5.13: Dust evolution for porous growth followed by erosion, in a compact $0.01 M_\odot$ disk with $\alpha = 10^{-3}$ and $Z_0 = 0.02$ (same model as Fig. 5.11). Times/locations where the mass-dominating particles have $10^{-3} \leq \Omega t_s \leq 1$ have been colored green, and the contours depict $(\rho_d^*/\rho_g)_{z=0} = \{0.1;0.5;1\}$.

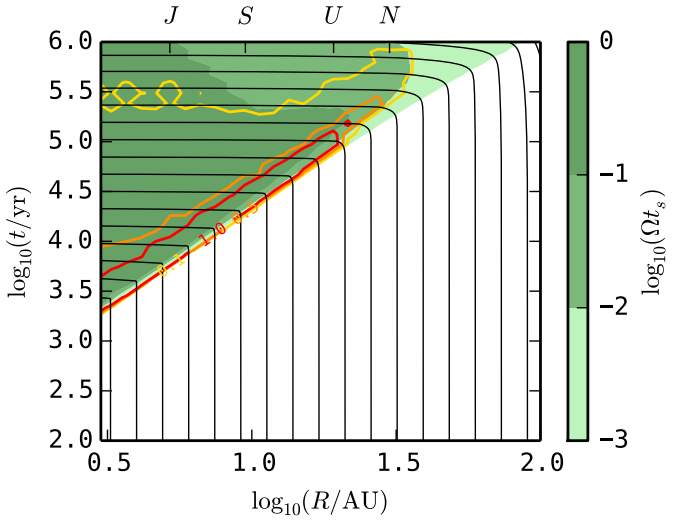

Figure 5.14: Same as Fig. 5.13, but using $\alpha = 10^{-5}$ and $Z_0 = 0.05$. The lower turbulence strength results in slower growth, but allows a higher mass loading in the midplane. Contours depict $(\rho_d^*/\rho_g)_{z=0} = \{0.1;0.5;1\}$.

Porous coagulation followed by drift-induced erosion however, is a robust way of creating *and keeping* a large amount of mass in aggregates with Stokes numbers around unity. This is illustrated in Fig. 5.13. The limiting criterion now becomes condition *ii)*: a dense midplane layer of solids. From Fig. 5.13 we learn that a turbulence strength of $\alpha = 10^{-3}$ at most results in a midplane dust-to-gas ratio of ∼0.1, about a factor of 10 too low. In Fig. 5.14, we have lowered the strength of the turbulence to $\alpha = 10^{-5}$, and increased the initial metallicity to $Z_0 = 0.05$. For this extreme case, we see that a region exists where conditions *i)*, *ii)*, and *iv)* are all met. The conditions are first met in a region in the inner disk after a few 10^3 yr, after which this region moves outward, reaching the current location of Uranus after 10^5 yr. In this 'front', marked by the red contour, we would expect SI to occur, and planetesimals to be formed locally.

5.4.4 Midplane turbulence

However, we cannot choose arbitrarily small values for α: the presence of decoupled particles can lead to Kelvin-Helmholtz instability (KH) and SI, and will give rise to a turbulence with strength (Takeuchi et al. 2012)

$$\alpha_{\rm mp} = \left[(C_1 C_{\rm eff}\eta Z)^{-2/3} + (C_2 C_{\rm eff}\eta/Z)^{-2}\right]^{-1} \Omega t_s, \tag{5.16}$$

where $C_1 = 1$, $C_2 = 1.6$, $C_{\rm eff} = 0.19$, η is given by Eq. 5.9, and $\Omega t_s < 1$ is the Stokes number of the mass-dominating particles responsible for the instability. For the disk models used in this work, $\alpha_{\rm KH} \simeq 10^{-6}$ and 10^{-4} in the inner disk for $\Omega t_s = 10^{-2}$ and 1 respectively (depending slightly on the metallicity Z), and increases by about a factor of 10 towards the outer disk. The turbulence strength obtained in Eq. 5.16 can be used as a minimum value for the turbulence, i.e., $\alpha \geq \alpha_{\rm mp}$. Making use of Eq. 5.13, we can then constrain the maximum midplane dust-to-gas ratio as

$$Z^*(h_g/h_d) \sim Z^*(\Omega t_s/\alpha)^{1/2} \leq Z^*(\Omega t_s/\alpha_{\rm mp})^{1/2}, \tag{5.17}$$

where we have used that $h_d/h_g \sim (\alpha/\Omega t_s)^{1/2}$ for high Stokes numbers (see Eq. 5.12). From Eq. 5.16 we find $\alpha_{\rm mp} \propto \Omega t_s$, so the dependence on particle Stokes number drops out of the expression for the maximum midplane mass loading, which is now a function only of the pressure profile η and metallicity Z^*.

Fig. 5.15 shows the midplane dust-to-gas ratio for different metallicities and disk models, assuming that the turbulence strength is given by Eq. 5.16 and the mass-dominating particles have been able to reach $10^{-2} \leq \Omega t_s \leq 1$. The figure shows that in order to reach the required dust-to-gas ratio in the midplane of an MMSN disk (upper panel), despite the turbulence triggered in the midplane, one needs a local metallicity (of high Stokes-number particles) of $Z^* = 0.03$ in the inner ∼10 AU, and $Z^* = 0.05$ in the region out to 80 AU. This indicates that, for a given metallicity, SI is easier to trigger at *smaller* radii. The reason can be understood as follows; if $\alpha_{\rm mp}$ is the main source of turbulence, the height of the dust layer is approximately $h_g/h_d \sim \eta v_{\rm K}/c_s \sim c_s/v_{\rm K} \sim h_g/R$. In other words, the relative height of the dust layer scales with the opening angle of the disk. In the MMSN

disk model, $h_g/R \propto R^{1/4}$, and disks with $\gamma = 1$ are flaring as well. As a result, creating a dense midplane layer of solids appears easier in the inner disk.

For a more extended disk with a shallower surface density profile (middle panel), the results are similar, and $Z^* = 0.03$ and $Z^* = 0.05$ result in $(\rho_d^*/\rho_g)_{z=0} \leq 1$ in the inner ~20 and 90 AU respectively. Since rapid porous growth followed by erosion results in an inside-out clearing of the dust in the disk (Fig. 5.11), pile-ups will not occur in the smooth disks considered in this work, and the only way to reach such high local metallicities is to start out with a super-Solar Z_0. A possible solution might be to lower the disk's temperature. The temperature structure used so far (Eq. 5.2) is based on an optically thin disk. However, (midplane) temperatures in disks might be significantly lower, especially if the disk is optically thick (e.g., Andrews et al. 2009). In a colder disk η will be smaller, reducing the strength of the midplane instability, and making it easier to form a dense midplane layer. The bottom panel of Fig. 5.15 uses $R_c = 100$ AU, and disk temperature that is reduced by 50% with respect to Eq. 5.2. In this relatively cold disk, $Z^* = 0.02$ could be enough to trigger SI in the inner 10 AU, and $Z^* = 0.03$ suffices out to 50 AU (provided there is no stronger source of turbulence present). However, in colder disks the maximum drift velocity is lower as well, possibly reducing the efficiency of erosion.

5.5 Discussion

5.5.1 Dust batch approach

The numerical method used in this work (Sect. 5.2.2), in which batches of dust are followed as they grow and drift in the protoplanetary nebula, provides an intuitive and flexible way to calculate (local) porous coagulation and the evolution of the global surface density simultaneously. Growth-limiting collisional processes such as bouncing, erosion and fragmentation can be incorporated in an straightforward manner. The flexibility and speed of this approach allow us to calculate a large number of models, and to study the impact of variations in parameters quickly by exploring a large parameter space while preserving the essential characteristics of the growth process. The method can readily be extended to more complicated gas disks. For example, rather than using a static and smooth $\Sigma_g(R)$, the method could be extended to deal with more complex $\Sigma_g(R, t)$, based on simulations of MRI turbulence, zonal flows, and embedded planets (e.g., Raettig et al. 2013; Uribe et al. 2013; Dittrich et al. 2013; Flock et al. 2015).

The method has two main drawbacks. First, it traces only the mass-dominating particles, and does not provide information about the number distribution for smaller masses. If the distribution can be assumed to be in growth/fragmentation equilibrium, the complete mass distribution may be reconstructed (e.g., Birnstiel et al. 2011), though this has not yet been attempted for porous growth, or for a steady state between growth and erosion. Second, in cases where drift is rapid (i.e., high $\dot{r}$), the radial distances between successive batches are increased. Because we use the radial distribution of the batches to obtain the dust surface density, the determination of $\Sigma_d(R)$ becomes less accurate in regions where few batches are present. A solution could be to simply increase the number

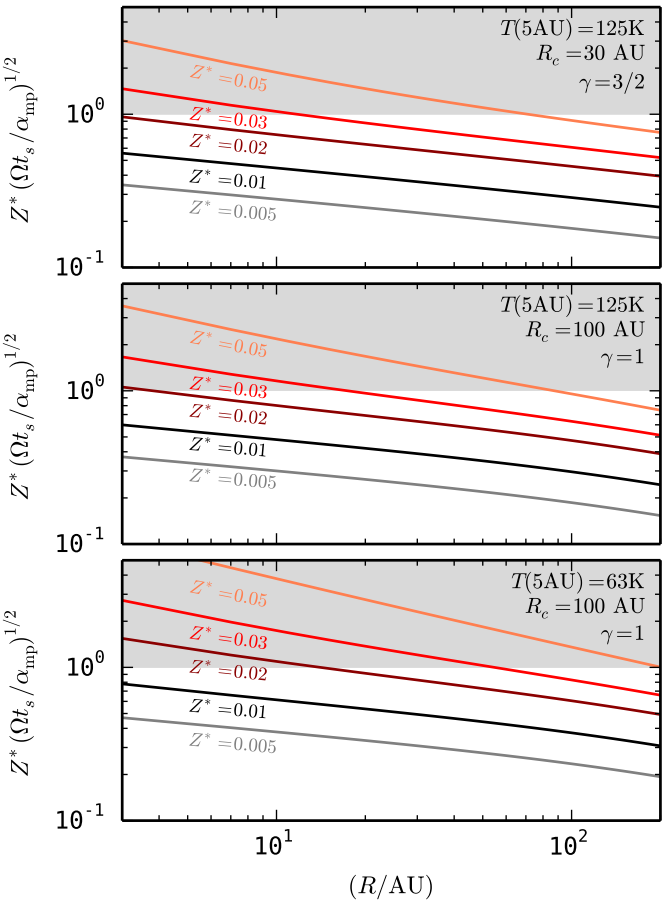

Figure 5.15: Midplane dust-to-gas ratio assuming the turbulence strength is given by Eq. 5.16, and the mass-dominating particles have $10^{-2} \leq \Omega t_s \leq 1$, for an MMSN-like disk (upper panel), a larger and shallower disk (middle panel), and a colder disk (bottom panel). Colors correspond to different metallicities, ranging from $0.5-5\times$ Solar. The grey shaded area indicates conditions necessary for planetesimal formation through SI.

of batches. Alternatively, if one is interested in a particular disk region or epoch, the initial radial distribution r_i could be chosen such to achieve highest numerical resolution in that region. Because we are mainly interested in the sites where planetesimals can form, i.e., places where Σ_d is high, our results are not affected by these issues.

5.5.2 Direct coagulation

In Sect. 5.3, we applied the method to study compact and porous coagulation behind the snow line. For compact particles, we considered a fragmentation threshold velocity of

several m s^{-1}, and found that growth beyond a cm in size is always impeded by fragmentation or radial drift (Fig. 5.3). However, there are still possibilities for compact grains to grow larger. If particles are sufficiently 'lucky', and participate only in relatively low-velocity collisions, they could potentially grow by effectively sweeping up small particles (Windmark et al. 2012a,b; Garaud et al. 2013; Drążkowska et al. 2014).

For porous icy aggregates however, fragmentation occurs only at very high velocities (Wada et al. 2013), and these fluffy aggregates can grow through the radial drift barrier. Rapid growth is harder to achieve in the outer disk, since timescales are longer and dust and gas spatial densities are lower. As a result, planetesimals form in a zone confined to the inner ~10 AU. Figs. 5.9 and 5.10 show how the size of this region depends on disk mass, temperature, and initial metallicity. Comparing the planetesimal formation zone to the current locations of the Solar System planets, we find that it is hard to form planetesimals out to the current location of Neptune. In the *Nice* model however, the giant planets of the Solar System were originally located much closer in, roughly between 5 and 17 AU, migrating out at later times (Tsiganis et al. 2005; Morbidelli et al. 2005; Gomes et al. 2005). At these locations[2], direct planetesimal formation through porous growth can be achieved, albeit only for relatively massive or cold disks. The calculations in Sect. 5.3 indicate the planetesimal surface density is highest near the outer boundary of the planetesimal zone. One could envision a scenario where enough material accumulates to trigger the formation of Jupiter early on. At that point, the assumptions in our model break down and the presence of Jupiter will steer the evolution of the disk and planet formation therein (e.g., Pollack et al. 1996; Pinilla et al. 2012a; Kobayashi et al. 2012).

The efficiency with which dust is converted into planetesimals can be very high, reaching up to 90% within 10^6 yr for relatively compact and dust-rich disks (Fig. 5.8). When the full mass distribution is taken into account, this efficiency will be lowered slightly, depending on how much mass is present in the low-mass end of the distribution. This picture of efficient dust-to-planetesimal conversion on a Myr timescale is consistent with the findings of Najita & Kenyon (2014), who, by comparing masses and locations of detected exoplanets to measured reservoirs of solids in T Tauri disks, concluded that a large fraction of the available solids has to be either hidden in the inner parts of the protoplanetary disk, and/or efficiently converted into large objects, avoiding detection.

Lastly, in the semi-analytical model of Sect. 5.2, planetesimals and dust do not interact with each other: the planetesimals do not contribute to the surface density of Eq. 5.10, and they do not sweep up drifting dust particles. As a result, aggregates that drift in at later times can drift *through* the planetesimal zone unaffected, as observed in Figs. 5.5 and 5.6. These conditions, a belt of planetesimals in the inner disk, and a reservoir of dust drifting in from the outer disk, are the starting conditions for pebble accretion[3] (Ormel & Klahr 2010; Lambrechts & Johansen 2012, 2014; Kretke & Levison 2014). If efficient, pebble accretion would result in an even higher planetesimal formation efficiency, since the mass present in the outer disk (which is substantial for large R_c) will be added to the

[2]The cores of the terrestrial planets require a different formation mechanism, as their close distances to the Sun do not allow the presence of sticky ices in their formation zone.

[3]Although the drifting particles in Fig. 5.6 are much larger and much more porous than the word 'pebble' would suggest.

planetesimals. However, the filtering of dust by planetesimals is not necessary efficient, depending on the turbulence strength and planetesimal characteristics (Guillot et al. 2014).

5.5.3 Streaming Instability

In Sect. 5.4, we investigated for which disk parameters compact and porous growth might lead to conditions favorable for triggering SI (Sect. 5.4.1), as defined by Drążkowska & Dullemond (2014). We found that porous growth followed by erosion (unlike compact growth followed by bouncing or fragmentation) naturally leads to a population of aggregates with Stokes numbers $10^{-2} \leq \Omega t_s \leq 1$ in a large portion of the protoplanetary disk. The most difficult condition to fulfill is then the creation of a dense midplane layer of solids. While this is possible for disks with a high metallicity and relatively weak turbulence (Fig. 5.14), the presence of the decoupled dust aggregates will lead to a turbulence that can be parametrized by Eq. 5.16 (Takeuchi et al. 2012), placing a lower limit on the local metallicity needed to achieve a dust-to-gas ratio of unity in the midplane. In that sense, condition *iii)* of Sect. 5.4.1 is not so much a separate criterion, but can be thought of as a prerequisite for criterion *ii)* in the presence of strong midplane turbulence.

For MMSN-like disks, and disks with a shallower profile (Upper and middle panel of Fig. 5.15), this lower limit is $Z^* \sim 0.03$ in the inner ~10 AU, and even higher in the outer disk. Since we only consider smooth disks, and porous growth leads to an inside-out clearing of the dust, pile-ups (as seen in Fig. 5.1) are not created and the only way to achieve these desired metallicities is to start from a high initial metallicity Z_0. For colder disks, a metallicity of $Z^* = 0.02$ might suffice to create a dense midplane layer inside of 10 AU. However, in colder disks the maximum drift velocity ηv_K is reduced as well, making the process of erosion less efficient. Without strong erosion, particles readily grow to larger Stokes numbers in the inner disk, not fulfilling condition *iv)* of Sect. 5.4.1.

We have employed a vertically isothermal disk, described by a simple temperature power-law. In reality, the midplane will be colder than the disk upper layers, and its temperature sensitive to the dust opacities (e.g., Min et al. 2011). To fully appreciate the interplay between porous growth, erosion, and SI, future models will have to self-consistently model the full particle mass- and porosity-distribution as it evolves through coagulation and erosion, while taking into account the feedback of the particles onto the gas. For example, small grains will influence the local temperature, and the massive, marginally decoupled grains can trigger Kelvin-Helmholtz instability or SI. In addition, when clumping through SI occurs, the collision velocities inside the clumps can be lowered (e.g., Bai & Stone 2010a), possibly altering the dominant collisional outcomes.

Observations show clear evidence for small dust grains in relatively old disks (e.g., Birnstiel et al. 2009). Thus, any mechanism that is capable of efficiently converting dust in to planetesimals (be it rapid porous growth, or SI) must not be too efficient, i.e., a population of small grains has to has to be sustained for over $\sim 10^6$ yr. In the outer parts of weakly turbulent disks, fragmenting collisions between similar-size aggregates are not expected to occur, though some mass loss may occur even in 'sticking' collisions (Wada et al. 2013, Sect. 4.3). In these regions, erosive collisions (i.e., high-speed collisions between aggregates with a high mass ratio) might be a way to keep a population of small

grains around; a population that is removed quickly when *all* collisions result in perfect sticking (Dullemond & Dominik 2005). To study these issues, models that resolve the full mass distribution are necessary.

5.5.4 Planetesimal characteristics and further evolution

Focussing on the growth towards planetesimals, we stopped following the planetesimals when they reached masses of $m \geq 10^{16}$ g, and described the planetesimal populations only in terms of their total mass, without specifying the properties of the individual planetesimals. An interesting question is how the considered formation mechanisms (direct coagulation and SI) affect the internal structure and composition of the formed planetesimals.

Focussing on the mechanical properties first, we see from Fig. 5.5 that the coagulated planetesimals are fairly compact, $\phi \sim 10^{-1}$, despite their highly porous history. This relatively high internal density is the result of self-gravity compaction, not of collisional compaction (Kataoka et al. 2013b; Krijt et al. 2015). Skorov & Blum (2012) and Blum et al. (2014) argue that the tensile strengths of planetesimals formed out of direct coagulation of (sub)micron-size icy monomers are too large to explain the activity of comets at relatively large separations from the Sun, and conclude that a gravitational collapse of larger, mm-sized particles is more in line with the observed cometary activity. However, the porous aggregates capable of triggering SI in Sect. 5.4 are much larger and more porous than mm-sized pebbles, and it is not clear what the mechanical properties would be of a planetesimal formed out of their collapse. Nonetheless, studying the internal mechanical structure of large bodies will certainly lead to a better understanding of their formation history.

Second, the composition of the planetesimals might well be different for both formation mechanisms. Fig. 5.6 shows that the planetesimals, even though they form exclusively inside of 5 AU, contain material that was originally located between $\sim 3 - 60$ AU. As the disk's temperature and chemical structure shows significant variations at these (length-)scales, we can expect information about these variations to be locked up in the planetesimals. The formation of planetesimals through SI should lead to 'local' planetesimals; while the zone where SI-conditions are reached in Fig. 5.14 moves outward in time, it preferentially contains dust batches that originate from very close by.

5.6 Conclusions

We have developed a novel approach for calculating the evolution of the mass-dominating dust aggregates as they grow and drift in a protoplanetary disk. The dust population is described by a collection of dust batches, each one containing a mono-disperse dust population, which can move through the disk as a result of radial drift. The method allows the calculation of the global evolution of the dust surface density on Myr timescales, while preserving the essential characteristic of the porous growth process. The method is fast

and flexible, and can be readily extended to include more complex or time-dependent gas disk models.

We have used the method the study the formation of the first generation of planetesimals - the one that is capable of forming out of a smooth gaseous nebula - in disks around Sun-like stars. When fragmentation and erosion are inefficient, planetesimals can form through porous coagulation in the inner ∼10 AU (Okuzumi et al. 2012). In these cases:

1. Planetesimals form between $\sim 10^3$ and 10^5 yr for $\alpha = 10^{-3}$, and can include material that originates from very far out in the disk (Fig. 5.6). In more extended disks ($R_c = 100$) and disks with a weaker turbulence, the timescales for planetesimal formation are increased.

2. Planetesimal formation is very efficient, with a large fraction of the initial dust content of the disk ending up in planetesimals (Figs. 5.7 and 5.8). Relatively compact and dust-rich disks have the highest planetesimal formation efficiency, converting up to 90% of their dust into planetesimals within a million years.

3. The extent of the planetesimal formation zone depends on the total disk mass and metallicity (Fig. 5.9) and the disk temperature structure (Fig. 5.10). Massive disks ($0.2 M_\odot$) that are dust-rich ($Z_0 = 0.05$) or relatively cold, can form planetesimals out to 20 AU.

Alternatively, when erosion balances growth around $\Omega t_s \sim 1$ (Krijt et al. 2015), further coagulation is not possible, but conditions necessary for streaming instability (SI) might be reached. While for compact growth, terminated by bouncing/fragmentation at a collision velocity of ∼m s^{-1}, maximum Stokes numbers lie below $\Omega t_s \sim 10^{-2}$ (Fig. 5.12 and Drążkowska & Dullemond 2014), we find that:

4. Porous growth limited by drift-induced erosion is an effective way of creating aggregates with $10^{-2} \leq \Omega t_s \leq 1$ in a large region of the disk (Figs. 5.13, 5.14 and Krijt et al. 2015).

5. In a smooth gas disk, the most stringent condition for triggering SI is creating and maintaining a dense midplane layer of solids. We find both a high initial metallicity ($Z_0 = 0.05$) and low turbulence strength ($\alpha = 10^{-5}$) are needed to create such a layer. In such cases, a dense midplane layer (with a dust-to-gas ratio ≥1) will first form in the inner disk after several kyr, and then move out in time (Fig. 5.14).

6. When KH and SI give rise to a midplane turbulence given by Eq. 5.16, we can calculate the local metallicity that is needed to reach a mass loading of unity in the midplane (Fig. 5.15). We find that for typical disks, a super-Solar metallicity is needed ($Z^* \geq 0.03$), with the highest midplane density being reached at small radii. For example, for $Z^* = 0.03$, the region where $(\rho_d^*/\rho_g)_{z=0} \geq 1$ extends out to 10 AU. For colder disks, $Z^* = 0.02$ suffices in the inner 10 AU.

7. For a smooth disk profile, rapid porous growth followed by erosion leads to an inside-out clearing of the dust disk (Fig. 5.11). In such a scenario, no pile-ups are created, and the only way to reach high metallicities is to start out with them.

Acknowledgements

Dust studies at Leiden Observatory are supported through the Spinoza Premie of the Dutch science agency, NWO. S.K. would like to thank C.P. Dullemond, J. Drążkowska, and T. Birnstiel for encouraging discussions.

5.A Particle stopping time

The particle stopping time is a function of an aggregate's mass m and size a, and the properties of the local gas. Depending on the aggregate size in relation to a gas molecule mean free path $\lambda_{\rm map}$, the stopping time is given by the Epstein or Stokes drag regime through

$$t_s = \begin{cases} t_s^{(\rm Ep)} = \dfrac{3m}{4\rho_g v_{\rm th} A} & \text{for } a < \dfrac{9}{4}\lambda_{\rm mfp}, \\ t_s^{(\rm St)} = \dfrac{4a}{9\lambda_{\rm mfp}} t_s^{(\rm Ep)} & \text{for } a > \dfrac{9}{4}\lambda_{\rm mfp}, \end{cases} \tag{5.18}$$

with $v_{\rm th} = \sqrt{8/\pi} c_s$ the mean thermal velocity of the gas molecules. The mean free path depends on the gas density and is given by $\lambda_{\rm mfp} = m_g/(\sigma_{\rm mol}\rho_g)$, with $\sigma_{\rm mol} = 2 \times 10^{-15}$ cm^2 the molecular cross section. For porous aggregates, the cross section A equals the orientation-averaged projected cross-section Okuzumi et al. (2009).

Eq. 5.18 is valid when the particle Reynolds number $\mathrm{Re_p} = 4a v_{\rm dg}/(v_{\rm th}\lambda_{\rm mfp}) < 1$, with $v_{\rm dg}$ the relative velocity between the gas and the dust particle. For the largest bodies however, this condition is often not met. In these cases, it is useful to write the stopping time as

$$t_s = \frac{2m}{C_D \rho_g v_{\rm dg} A}, \tag{5.19}$$

with C_D the drag coefficient. Following Weidenschilling (1977a), we use

$$C_D = \begin{cases} 24(\mathrm{Re_p})^{-1} & \text{for } \mathrm{Re_p} < 1, \\ 24(\mathrm{Re_p})^{-3/5} & \text{for } 1 < \mathrm{Re_p} < 800, \\ 0.44 & \text{for } 800 < \mathrm{Re_p}. \end{cases} \tag{5.20}$$

For large Reynolds numbers, the stopping time depends the velocity relative to the gas, and one has to iterate to obtain t_s.

5.B Particle relative velocity

The relative velocity between particle 1 and particle 2 is obtained by adding various velocity sources quadratically. We take into account relative velocities arising from Brownian

motion, turbulence, radial drift, and azimuthal drift. The Brownian motion relative velocity is given by

$$\Delta v_{\rm BM} = \sqrt{\frac{8 k_{\rm B} T (m_1 + m_2)}{\pi m_1 m_2}}, \tag{5.21}$$

and depends only on the particle masses.

The turbulence-induced relative velocity between two particles with stopping times $t_{s,1}$ and $t_{s,2} \leq t_{s,1}$ has three regimes (Ormel & Cuzzi 2007)

$$\Delta v_{\rm turb} \simeq \delta v_g \times \begin{cases} {\rm Re_t}^{1/4}\, \Omega (t_{s,1} - t_{s,2}) & \text{for } t_{s,1} \ll t_\eta, \\ 1.4 \ldots 1.7 \left(\Omega t_{s,1}\right)^{1/2} & \text{for } t_\eta \ll t_{s,1} \ll \Omega^{-1}, \\ \left(\dfrac{1}{1+\Omega t_{s,1}} + \dfrac{1}{1+\Omega t_{s,2}} \right)^{1/2} & \text{for } t_{s,1} \gg \Omega^{-1}, \end{cases} \tag{5.22}$$

where $\delta v_g = \alpha^{1/2} c_s$ is the mean random velocity of the largest turbulent eddies, and $t_\eta = {\rm Re_t}^{1/2} t_L$ is the turn-over time of the smallest eddies. The turbulence Reynolds number ${\rm Re_t} = \alpha c_s^2 / (\Omega \nu_{\rm mol})$, with the molecular viscosity $\nu_{\rm mol} = v_{\rm th} \lambda_{\rm mfp}/2$.

The relative velocity from radial drift just equals $\Delta v_r = |v_{\rm drift}(\Omega t_{s,1}) - v_{\rm drift}(\Omega t_{s,2})|$, with the drift velocity given by Eq. 5.8. The azimuthal relative velocity is obtained in a similar way, as $\Delta v_\phi = |v_\phi(\Omega t_{s,1}) - v_\phi(\Omega t_{s,2})|$ with

$$v_\phi = -\frac{\eta v_{\rm K}}{1 + (\Omega t_s)^2}. \tag{5.23}$$

Finally, the total relative velocity is given by

$$v_{\rm rel} = \sqrt{(\Delta v_{\rm BM})^2 + (\Delta v_{\rm turb})^2 + (\Delta v_r)^2 + (\Delta v_\phi)^2}. \tag{5.24}$$

The particle stopping times and relative velocities are calculated in the midplane of the gas disk, as this is where most of the coagulation occurs.

5.C Particle porosity evolution

Initially, particles grow through low-energy hit-and-stick collisions. During this growth phase, the fractal dimension $D_f \simeq 2$, and the porosity is given by

$$\phi \simeq (m/m_0)^{1/2}. \tag{5.25}$$

The fractal growth regime ends when collisions become energetic enough for compaction, or when gas ram pressure compaction becomes effective. Collisional compaction occurs when the kinetic energy in a (same-size) collision exceeds the critical rolling energy $E_{\rm roll}$ (Dominik & Tielens 1997). Based on experimental investigations (Heim et al. 1999; Gundlach et al. 2011) and theoretical work (Krijt et al. 2014) we use

$$E_{\rm roll} = \left(\frac{a_0}{1\ \mu{\rm m}} \right)^{5/3} \times \begin{cases} 1.8 \times 10^{-7}\ {\rm erg} & \text{for ice particles,} \\ 8.5 \times 10^{-9}\ {\rm erg} & \text{for silicate particles.} \end{cases} \tag{5.26}$$

If the collisional energy E_K exceeds the critical energy for rolling, we make use of Eq. 31 of Okuzumi et al. (2012), which, depending on the turbulent velocity regime, predicts how the internal density (which is proportional to ϕ) scales with increasing particle mass. In practice, collisional compaction results in the porosity staying roughly constant in the regime where $E_K > E_{roll}$ (Okuzumi et al. 2012).

For low internal densities, Kataoka et al. (2013b) found that the external pressure a dust aggregate can just withstand equals

$$P_c = \frac{E_{roll}}{a_0^3}\phi^3. \tag{5.27}$$

This pressure can then be compared to the pressure arising form the surrounding gas and from self-gravity (Kataoka et al. 2013a)

$$P_{gas} = \frac{v_{dg}m}{\pi a^2 t_s}, \qquad P_{grav} = \frac{Gm^2}{\pi a^4}, \tag{5.28}$$

with G the gravitational constant.

In our semi-analytical model, we start by assuming fractal growth according to Eq. 5.25. At every increase in mass, we check *i)* if the energy in same-size collisions exceeds the critical energy for rolling, and *ii)* whether gas- or self-gravity compaction are expected. This involves calculating the stopping time, and relative collision velocity as a function of the current location in the gas disk. If collisional compaction is expected we make use of Eq. 31 of Okuzumi et al. (2012), and calculate the new porosity from the previous one. If gas- or self-gravity compaction are important we calculate $\phi(m)$ by setting Eq. 5.27 equal to Eq. 5.28.